

Inhibition of KIF20A suppresses the replication of influenza A virus by inhibiting viral entry

Hoyeon Jeon¹, Younghyun Lim¹, In-Gu Lee¹,
Dong-In Kim¹, Keun Pil Kim¹, So-Hee Hong²,
Jeongkyu Kim^{1*}, Youn-Sang Jung^{1*},
and Young-Jin Seo^{1*}

¹Department of Life Science, Chung-Ang University, Seoul 06974, Republic of Korea

²Department of Microbiology, College of Medicine, Ewha Womans University, Seoul 07804, Republic of Korea

(Received Sep 28, 2022 / Revised Oct 11, 2022 / Accepted Oct 12, 2022)

The influenza A virus (IAV) has caused several pandemics, and therefore there are many ongoing efforts to identify novel antiviral therapeutic strategies including vaccines and antiviral drugs. However, influenza viruses continuously undergo antigenic drift and shift, resulting in the emergence of mutated viruses. In turn, this decreases the efficiency of existing vaccines and antiviral drugs to control IAV infection. Therefore, this study sought to identify alternative therapeutic strategies targeting host cell factors rather than viruses to avoid infection by mutated viruses. Particularly, we investigated the role of KIF20A that is one of kinesin superfamily proteins in the replication of IAV. The KIF20A increased viral protein levels in IAV-infected cells by regulating the initial entry stage during viral infection. Furthermore, the KIF20A inhibitor significantly suppressed viral replication, which protected mice from morbidity and mortality. Therefore, our findings demonstrated that KIF20A is highly involved in the viral replication process and viral propagation both *in vitro* and *in vivo*, and could thus be used as a target for the development of novel antiviral drugs.

Keywords: influenza A virus, KIF20A, paprotrain

Introduction

Influenza A virus (IAV) causes acute respiratory inflammation in humans (Fukuyama and Kawaoka, 2011). Particularly, H1N1, a subtype of IAV, induces more pathogenic symptoms than other seasonal influenza viruses. Given that H1N1 caused a pandemic that resulted in 50 million deaths worldwide in 1918, various studies have sought to prevent another similar epidemic. However, IAVs undergo antigenic evolution

through antigenic drift and shift of surface glycoproteins (Kim *et al.*, 2018; Noh *et al.*, 2022), and therefore frequent updates of vaccine antigens are required to prevent the spread of continuously evolving IAV strains.

Intracellular transport systems deliver various molecules such as proteins and lipids to the proper sites. Motor proteins also participate in this process, thus shaping cell morphogenesis and influencing physiological functions (Miki *et al.*, 2001; Dodding and Way, 2011). Among these intracellular motor proteins, kinesin superfamily proteins (KIFs) are crucial components of the intracellular transport system that transport organelles, protein complexes, and mRNA by interacting with microtubules in an ATP-dependent manner. However, upon viral infection, viruses can take over the microtubule-mediated transport system of host cells to promote their replication and enhance propagation (Döhner *et al.*, 2005; Greber and Way, 2006; Radtke *et al.*, 2006; Brandenburg and Zhuang, 2007; Ward, 2011), suggesting that KIFs might be involved in IAV replication. In fact, KIF13A is known to play a crucial role in the transport of influenza A viral ribonucleoprotein (vRNP), which is an essential step in viral assembly (Ramos-Nascimento *et al.*, 2017). Moreover, previous studies have reported that IAV infection increases the expression of KIF11 and KIF18A, thus promoting the replication of IAVs (Cho *et al.*, 2020; Kim *et al.*, 2021).

KIF20A (mitotic kinesin-like protein 2; MKLP-2) regulates cell division via central spindle assembly and cleavage furrow formation (Liu *et al.*, 2013; Wu *et al.*, 2019). High expression levels of KIF20A have been linked to poor prognosis in cancer patients (Shen *et al.*, 2019; Nakamura *et al.*, 2020; Zhang *et al.*, 2020). KIF20A is thus a promising target for the development of prognostic biomarkers and anti-cancer therapeutics due to its known involvement in the enhancement of cell division via microtubule regulation. Additionally, KIF20A regulates porcine oocyte maturation and early embryo development (Zhang *et al.*, 2014). KIF20A knock-out mice exhibit embryonic lethality and loss of cortical neural progenitor cells (Geng *et al.*, 2018), which may be caused by impaired cytokinesis and anomalies during early embryonic development. These results suggest that KIF20A-controlled microtubule dynamics is involved in various physiological functions including defense against pathogen infection. A previous study confirmed that KIF20A expression increased in the lungs of IAV-infected mice (Qiu *et al.*, 2015). However, the function and involvement of this protein during viral replication remain unclear. Therefore, our study sought to reveal whether KIF20A contributes to IAV replication and investigated the effect of suppressing KIF20A activity on the morbidity and mortality of IAV-infected mice.

*For correspondence. (Y.J. Seo) E-mail: yjseo@cau.ac.kr; Tel.: +82-2-820-5925; Fax: +82-2-825-5925 / (Y.S. Jung) E-mail: younsang@cau.ac.kr; Tel.: +82-2-820-5375; Fax: +82-2-825-5925 / (J. Kim) E-mail: kimj@cau.ac.kr; Tel.: +82-2-820-5353; Fax: +82-2-825-5925

Copyright © 2022, Author(s) under the exclusive license with the Microbiological Society of Korea

Materials and Methods

Virus, cells, and infection

Influenza A/California/04/2009 (H1N1) virus was kindly provided by Dr. Eui Ho Kim (Institut Pasteur Korea). Amplification and titration of the virus were performed on Madin-Darby Canine Kidney (MDCK) cells. MDCK cells were maintained in Eagle's minimum essential medium (MEM, GenDEPOT) supplemented with penicillin/streptomycin (GenDEPOT) and 10% fetal bovine serum (FBS, GenDEPOT). Human embryonic kidney (HEK) 293 cells were maintained in Dulbecco's modified Eagle's medium (DMEM, GenDEPOT) supplemented with penicillin/streptomycin and 10% FBS. To infect the cells, MDCK or HEK293 cells were incubated with influenza virus for 1 h in the presence of MEM or DMEM with 0.3% bovine serum albumin (BSA) and TPCK-trypsin (2 µg/ml, Sigma-Aldrich).

Chemicals

A KIF20A inhibitor (paprotrain, > 97%) was purchased from Tocris Bioscience, and oseltamivir phosphate (> 98%) was purchased from Sigma-Aldrich.

Plasmid and transfection

For KIF20A overexpression, the KIF20A clone (KU004860) was provided by the Korea Human Gene Bank, Medical Genomics Research Center, KRIBB, Korea. Afterward, the KIF20A coding sequence was cloned into the C-terminus of the cytomegalovirus (CMV) promoter-driven green fluorescent protein (GFP) reporter expression vector. The cells were then transfected using the Lipofectamine™ 3000 reagent (Invitrogen) according to the manufacturer's instructions. Transfection efficiency and transgene expression levels were measured by quantifying the fluorescent signal of the GFP reporter from the chimeric GFP-KIF20A protein via flow cytometry or fluorescent microscopy.

Real-time quantitative PCR (qRT-PCR)

HEK293 cells were infected with IAV for 6 h at a multiplicity of infection (MOI) of 1. Total RNA was extracted using NucleoZOL (Bio-Medical Science) for cDNA synthesis using the ReverTraAce qPCR RT kit (Toyobo). qRT-PCR for viral RNAs (Matrix protein 1; M1, Nucleoprotein; NP) and KIF20A was performed using a CFX Connect real-time system (Bio-Rad) using the following primers: GAPDH, forward 5'-TGG ACC TGA CCT GCC GTC TA-3' and reverse 5'-CCC TGT TGC TGT AGC CAA ATT C-3'; M1, forward 5'-AAG ACC AAT CCT GTC ACC TCT G-3' and reverse 5'-CAA AAC GTC TAC GCT GCA GTC C-3'; NP, forward 5'-CCA GAT CAG TGT GCA GCC TA-3' and reverse 5'-CTT CTG GCT TTG CAC TTT CC-3'; KIF20A, forward 5'-ACC AGC AGA ACC GGT CAA AG-3' and reverse 5'-GCC TCG GCC TGT GAA GAA AC-3'; interleukin-6 (IL-6) for mouse, forward 5'-AC GGCCTTCCCTACTTCACA-3' and reverse 5'-CATTTCC ACGATTTCCCGA-3'; tumor necrosis factor-alpha (TNF-α) for mouse, forward 5'-GCC TCT TCT CAT TCC TGC TTG-3' and reverse 5'-CTG ATG AGA GGG AGG CCA TT-3'; interferon-gamma (IFN-γ) for mouse, forward 5'-GGC

CAT CAG CAA CAA CAT AAG CGT-3' and reverse 5'-TGG GTT GTT GAC CTC AAA CTT GGC-3'. qRT-PCR experiments were performed under the following conditions: 15 min at 95°C, followed by 40 cycles of 95°C for 20 sec, 55°C for 20 sec, and 73°C for 20 sec (Lim *et al.*, 2021).

Western blot analyses

Sample proteins were extracted using NP40 protein extraction solution (Elpisbio) and protease/phosphatase inhibitor (Thermo Scientific). Protein quantification was performed with the Pierce BCA protein assay kit (iNtRON Biotechnology). The same amount of protein (7–10 µg) was loaded onto SDS-PAGE gels (8% or 15%), after which the separated proteins were transferred to a nitrocellulose membrane. The samples were then blocked in 2% BSA solution and the membranes were then incubated with primary antibodies (1:500) overnight at 4°C, followed by incubation with secondary antibodies (1:5,000) at room temperature for 1 h. Next, the membrane was washed and visualized using the SuperSignal West Pico PLUS-enhanced chemiluminescent substrate (Thermo Scientific).

Immunofluorescence analysis

HEK293 cells were plated on a Poly-D-Lysine (Corning)-coated 4-well cell culture chamber slide (Millipore) and infected with IAV for the indicated time at an MOI of 3. After fixation and permeabilization, the cells were incubated with anti-influenza virus NP antibodies (1 µg/ml, Abcam) and then incubated with Alexa Fluor 488-conjugated secondary antibodies (Thermo Scientific). The cells were mounted with DAPI and Fluoroshield (Thermo Fisher). Images were obtained using a CKX53 (Olympus) cell culture microscope at 400x magnification. At least three fields were visualized for each slide.

Intracellular flow cytometry

To detect the expression of intracellular influenza viral proteins, cells were fixed and then permeabilized with Cyto-Fast™ Fix/Perm Buffer Set (Biolegend) according to the manufacturer's instructions. After fixation and permeabilization, anti-influenza viral M1 (5 µg/ml, Abcam) or NP antibodies (2.5 µg/ml, Abcam) were added, followed by staining with Alexa Fluor 647-conjugated secondary antibodies (10 µg/ml, Invitrogen). Data were collected using an Attune™ NxT Acoustic Focusing Cytometer (Thermo Scientific) and analyzed using the FlowJo software (BD Biosciences).

Plaque assay

For IAV titration, MDCK cells were plated in 6-well-plates. The next day, the cells were incubated with IAV-containing supernatant. After incubation for 1 h, the infected cells were covered with 1% SeaPlaque agarose diluted in MEM containing 0.3% BSA and TPCK. Three days later, the cells were fixed with 3.5% formaldehyde solution. The cells were stained with 1% crystal violet (Sigma) dye solution at room temperature for 10 min and rinsed with PBS to remove excess dye. Plaques were visible when dead cells were present due to IAV infection.

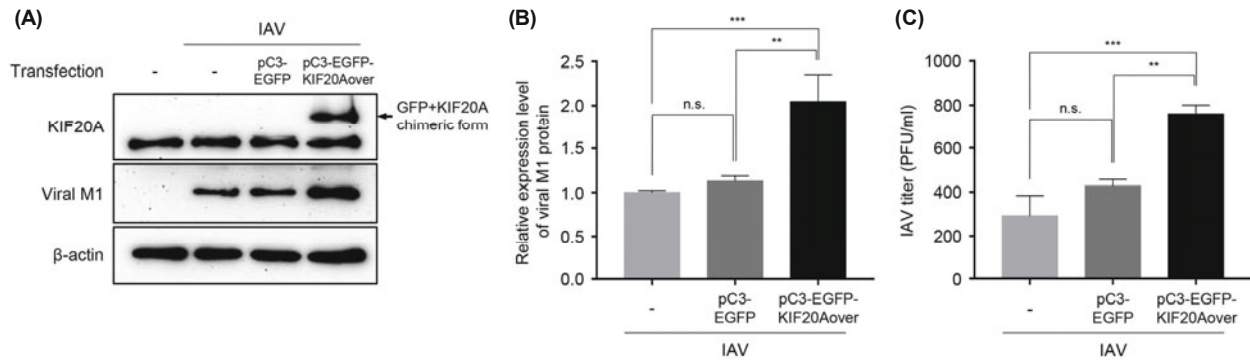


Fig. 1. KIF20A overexpression increases the expression of IAV protein. The pC3-EGFP control vector and pC3-EGFP-KIF20A overexpression vector were transfected into HEK293 cells. At 24 h after transfection, HEK293 cells overexpressing KIF20A were infected with IAV at an MOI of 1 and were harvested at 18 hpi. (A and B) The expression level of KIF20A, viral M1, and β-actin was analyzed by western blotting. (B) The relative intensities for each viral M1 band were determined based on β-actin by densitometric analysis. (C) IAV titers in the supernatants were measured by a plaque assay. Statistically significant differences between samples were analyzed via Student's *t*-test (n.s., not significant; ** $P < 0.01$, *** $P < 0.001$). Representative data of two independent experiments are shown.

Animals and *in vivo* infection

All animal experiments were performed in accordance with protocols approved by the Institutional Animal Care and Use Committee of Ewha Womans University (Approval No.: EWHA MEDIACUC 22-020). For infection, 7- to 8-week-old C57BL/6 mice were infected intranasally (i.n.) with 5×10^2 plaque forming units (PFUs)/mouse. At 10 min post-infection (mpi), 3 h post-infection (hpi), and 6 hpi, the mice were intranasally treated with DMSO or paprotrain solution (0.0025 mg/kg). Body weight was measured daily for 14 days.

Isolation of mouse lung cells and splenocytes

For the isolation of mouse lung cells, lungs were cut into pieces with scissors after injecting 500 μl of 2 mg/ml collagenase into each lobe. After the incubation for 15 min at 37°C, 4 μl of 0.5 M EDTA solution (Welgene) was added, and the samples were further incubated for 5 min at 37°C. Samples were

then filtered with 40 μm cell strainers. Following centrifugation, the cell pellets were treated with eBioscience™ RBC Lysis Buffer (ThermoFisher) for 4–5 min to remove red blood cells. After washing, the cell pellets were resuspended in 31.5% Percoll solution (GE healthcare). After centrifugation, the cell pellets were subjected to LPS or IAV stimulation. For the isolation of splenocytes, spleens were mashed in 40 μm cell strainers. After red blood cells were removed, splenocytes were resuspended in RPMI-1640 containing 10% FBS and penicillin/streptomycin for subsequent experiments.

Statistics

Mean values were compared using unpaired Student's *t*-tests, analysis of variance (ANOVA), or a log-rank test. Error bars indicate the standard error of the mean (SEM). Statistical analyses were conducted using the GraphPad Prism (v.7) software (GraphPad Software).

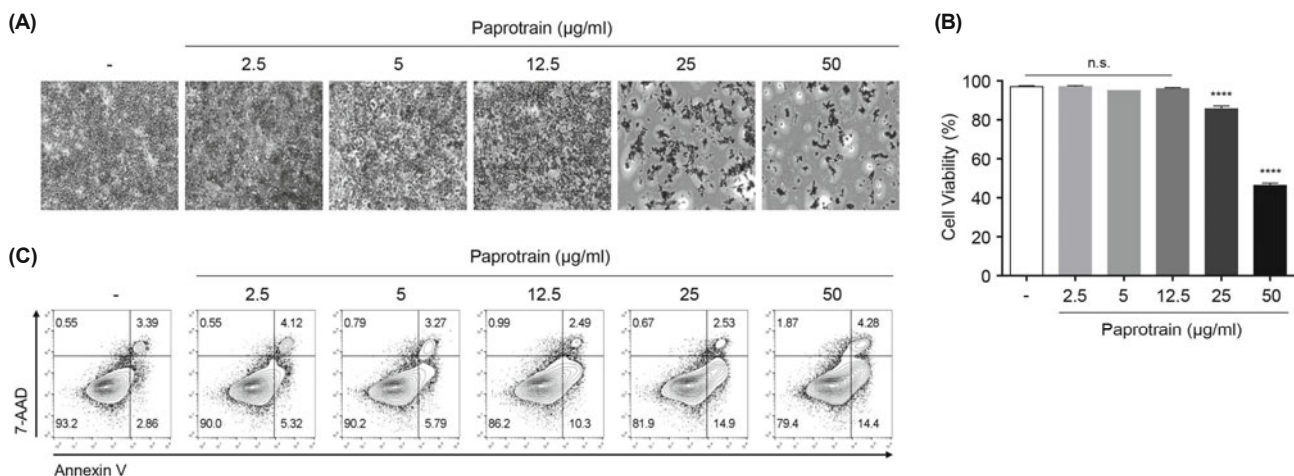


Fig. 2. Paprotrain decreases cell viability at concentrations above 25 μg/ml. HEK293 cells were treated with 2.5, 5, 12.5, 25, and 50 μg/ml of paprotrain for 24 h. (A) Cells were stained with CV after fixing with 4% formaldehyde. (B) Percentage of CV-stained live cells in (A). (C) Cells were stained with Annexin V/7-AAD and analyzed on a flow cytometer. (n.s., not significant; **** $P < 0.0001$) All experiments were conducted at least three times.

Results

KIF20A upregulates the expression of viral protein in HEK293 cells

Given that KIF20A is highly expressed in the lung of IAV-infected mice (Qiu *et al.*, 2015), we hypothesized that KIF20A plays a role in IAV replication. Thus, we sought to elucidate whether KIF20A upregulation affects viral replication. To this end, we employed a c-terminus GFP-tagged KIF20A. The pC3-EGFP vector was transfected into HEK293 cells to explore the effects of the CMV promoter in the plasmid on

IAV replication. While pC3-EGFP vector transfection did not notably change viral M1 expression level, ectopic expression of KIF20A strongly elevated the expression of viral M1 (Fig. 1A and B). Furthermore, we performed a plaque assay to quantitatively analyze the production of infectious viral particles. In agreement with the increased expression of viral M1 protein (Fig. 1A and B), a significant increase in IAV titers was observed when cells were overexpressed with KIF20A viral replication (Fig. 1C). Therefore, these results suggest that KIF20A may enhance viral replication. Based on this, we further hypothesized that viral protein replication can be suppressed when KIF20A is inhibited.

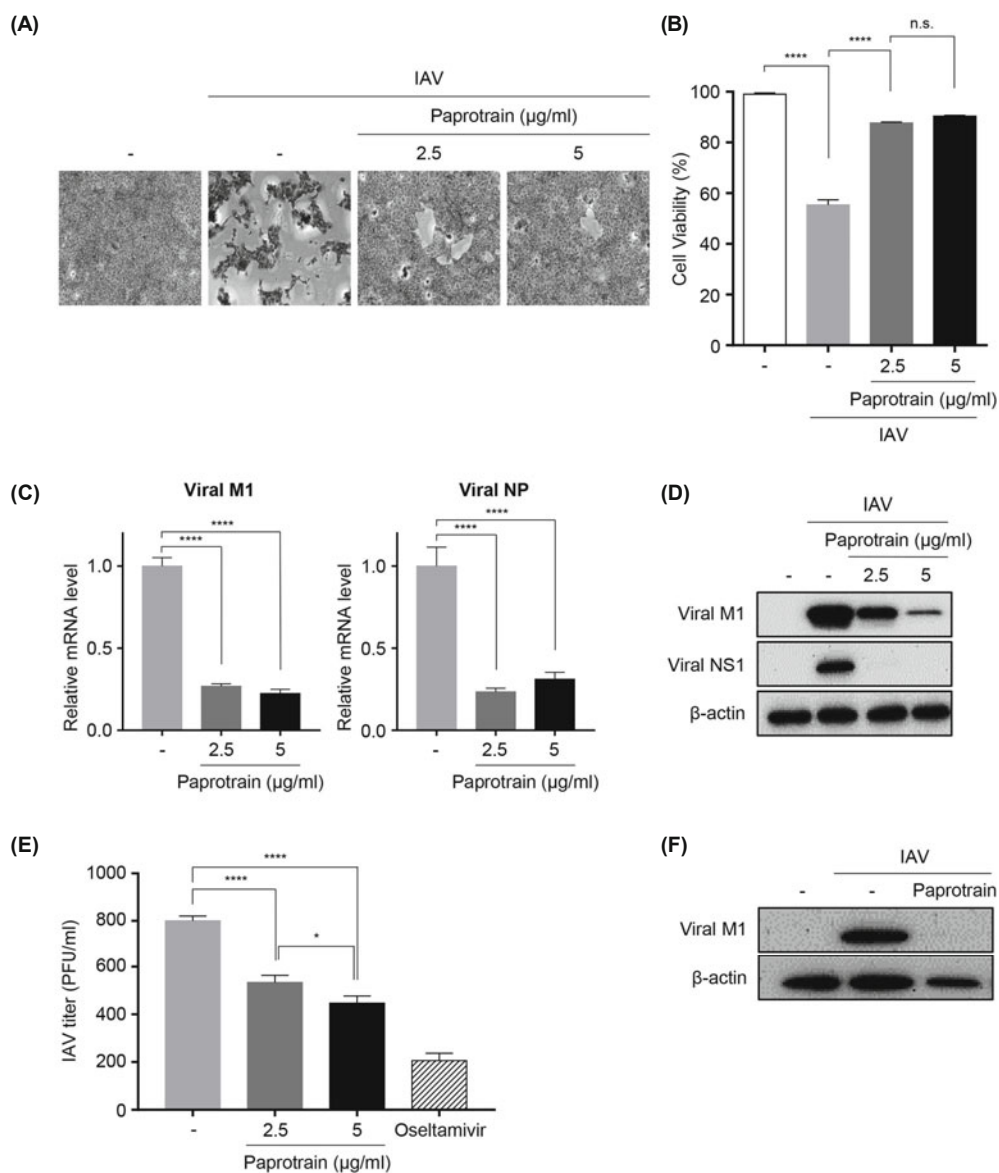


Fig. 3. KIF20A inhibitor treatment suppresses IAV replication. HEK293 cells were infected with an MOI of 0.1 and treated with paprotrain at 2.5 or 5 µg/ml (A–E) or osettamivir phosphate (10 µg/ml) (D). (A) At 24 hpi, the cells were stained with CV after fixation. (B) Ratios of the area of the stained live cells to the total area are shown as a result of (A). (C) Viral M1 and NP mRNA levels were quantified by qRT-PCR at 6 hpi. (D) The expression levels of viral M1, viral NS1, and β-actin were analyzed by western blotting. (E) IAV titers in the supernatants were measured by a plaque assay at 24 hpi. (F) MDCK cells were infected with an MOI of 0.1 and treated with paprotrain at 5 µg/ml. The expression levels of viral M1 and β-actin were analyzed by western blotting. Statistically significant differences between samples were analyzed by one-way ANOVA (* $P < 0.05$, **** $P < 0.0001$). All experiments were conducted at least three times.

KIF20A inhibition interferes with IVA replication

A functional study of KIF20A revealed that an ATPase defective form of KIF20A impairs chromosomal partitioning (Louw *et al.*, 2018). Given that the loss of KIF20A induces cell death including apoptosis and autophagy (Zhu *et al.*, 2020), we first monitored the cytotoxic effects of paprotratin that is cell-permeable inhibitor for KIF20A ATPase activity (Labrière *et al.*, 2016a, 2016b). Similar to a previous knockdown study (Zhu *et al.*, 2020), crystal violet (CV) staining demonstrated that paprotratin triggers cell death (Fig. 2A and B) at high doses (25 or 50 $\mu\text{g/ml}$). Similarly, when analyzed by Annexin V/7-AAD staining assay, high doses of paprotratin dramatically induced apoptosis (Fig. 2C). Based on these results, we determined the optimal concentrations of paprotratin (2.5–5 $\mu\text{g/ml}$) to test the effect of KIF20A inhibition on IAV infection. Next, we examined whether paprotratin affects IAV-induced cytopathic effects (CPEs). While IAV infection dramatically induced CPEs, paprotratin treatment significantly

protected cells from the CPEs (Fig. 3A and B). Because CPEs occur as a result of IAV replication, the decreases in CPE levels induced by paprotratin (Fig. 2A and B) were possibly due to an inhibition in viral replication. Considering that ectopic expression of KIF20A positively regulated the expression of viral protein (Fig. 1), we next estimated whether paprotratin decreases the expression of viral proteins. As expected, paprotratin treatment significantly reduced the transcription levels of viral M1 and NP (Fig. 3C) in a dose-dependent manner, which was further supported by the results of immunoblotting for Viral M1 and Viral NS1 (Fig. 3D). Furthermore, paprotratin decreased the production of infectious viral particles (Fig. 3E), which was comparable with the antiviral effect of oseltamivir. In addition, similar to our results with HEK293 cells, the KIF20A inhibitor strongly suppressed the viral protein expression in MDCK cells (Fig. 3F). Therefore, KIF20A is likely a proviral factor that promotes IAV replication.

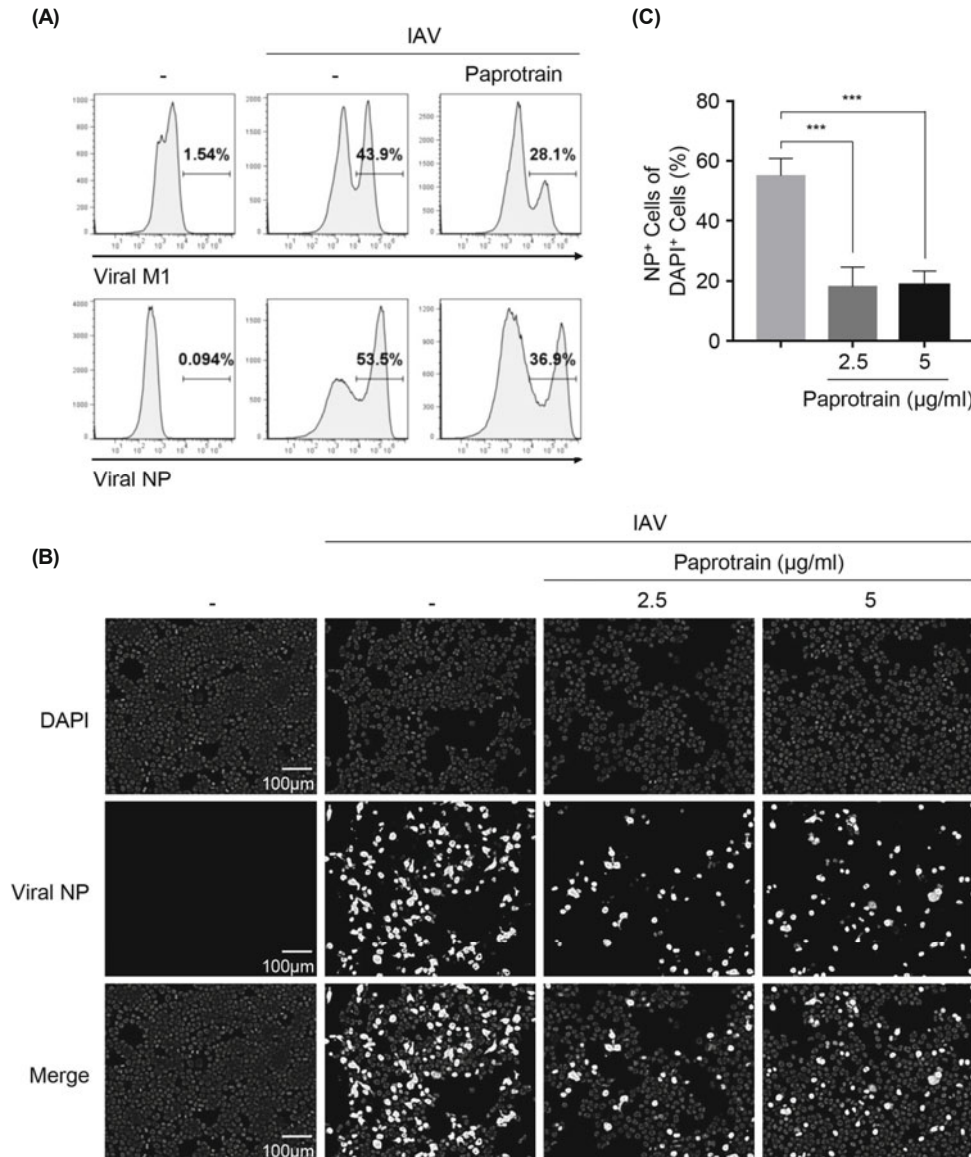


Fig. 4. Paprotratin reduces the percentage of infected cells in a single cell unit.

For single cell unit analysis, HEK293 cells infected with an MOI of 1 were treated with paprotratin and harvested at 24 hpi. (A and B) To measure intracellular viral protein expression, cells were subjected to fixation and permeabilization, and viral proteins were stained with Alexa Fluor-488-conjugated antibodies. (A) Stained viral M1 and NP were analyzed using a flow cytometer. (B) Viral NP (white) and nuclei (DAPI, gray) were observed at a 200 \times magnification using a fluorescence microscope. Representative images of at least three locations for each sample. (C) Ratio of cells expressing NP compared to total cells. Statistically significant differences between samples were analyzed by one-way ANOVA ($***P < 0.001$). All experiments were conducted at least three times.

KIF20A inhibitor reduces the proportion of IAV-infected cells

Although our findings confirmed that paprotrain reduced the total amount of viral protein, it is unclear whether paprotrain decreases the number of infected cells. To investigate the proportion of infected cells, we analyzed the expression of intracellular viral M1 and NP using a flow cytometer and immunofluorescence. The flow cytometric analysis indicated that paprotrain markedly downregulates the proportion of viral M1- and NP-positive cells compared to untreated cells (Fig. 4A; M1: 43.9% [untreated] vs. 28.1% [paprotrain-treated], NP: 53.5% [untreated] vs. 36.9% [paprotrain-treated]). Furthermore, immunofluorescence analyses demonstrated that paprotrain markedly decreased the number of viral NP-positive cells compared to untreated cells (Fig. 4B and C). Together, these results suggest that KIF20A inhibition reduced the number of IAV-infected cells.

KIF20A participates in the early entry process of IAV

IAVs require several stages to enter host cells (Luo, 2012). The first step is multivalent attachment, which is the recognition of host cell receptor molecules by hemagglutinin (HA). Multivalent attachment leads to endocytosis of IAVs through endosomes. Afterward, a unidirectional route transports the

endosome-trapped virus to the vicinity of the nucleus. Therefore, to examine the role of KIF20A in the entry process of IAV, we compared the expression levels of viral proteins by paprotrain treatment at each time point after IAV infection. Cells were treated with paprotrain at 0, 2, or 4 hpi. The expression of viral M1 was analyzed at 20 hpi. Interestingly, we found that paprotrain treatment at 0 or 2 hpi down-regulated the expression of viral M1, whereas treatment at 4 hpi did not (Fig. 5A). These results suggest that KIF20A is associated with the early stage of viral infection, which led us to further investigate the effect of paprotrain on viral attachment and the following entry step. First, cells were incubated with IAV in the presence of paprotrain at low-temperature infection (4°C) to allow viral attachment to the cell surface albeit without entering the cell. Second, cells were infected with IAV for 1 h, followed by immediate treatment with paprotrain for 2 h to test its effect on viral entry after attachment to the cell surface. Interestingly, viral M1 expression was not reduced when cells were treated with paprotrain during viral attachment. However, the amount of M1 was significantly decreased when the cells were treated with paprotrain at 0–2 hpi (Fig. 5B). These results indicate that paprotrain negatively regulates viral entry but not viral attachment on cells. Additionally, we examined whether paprotrain

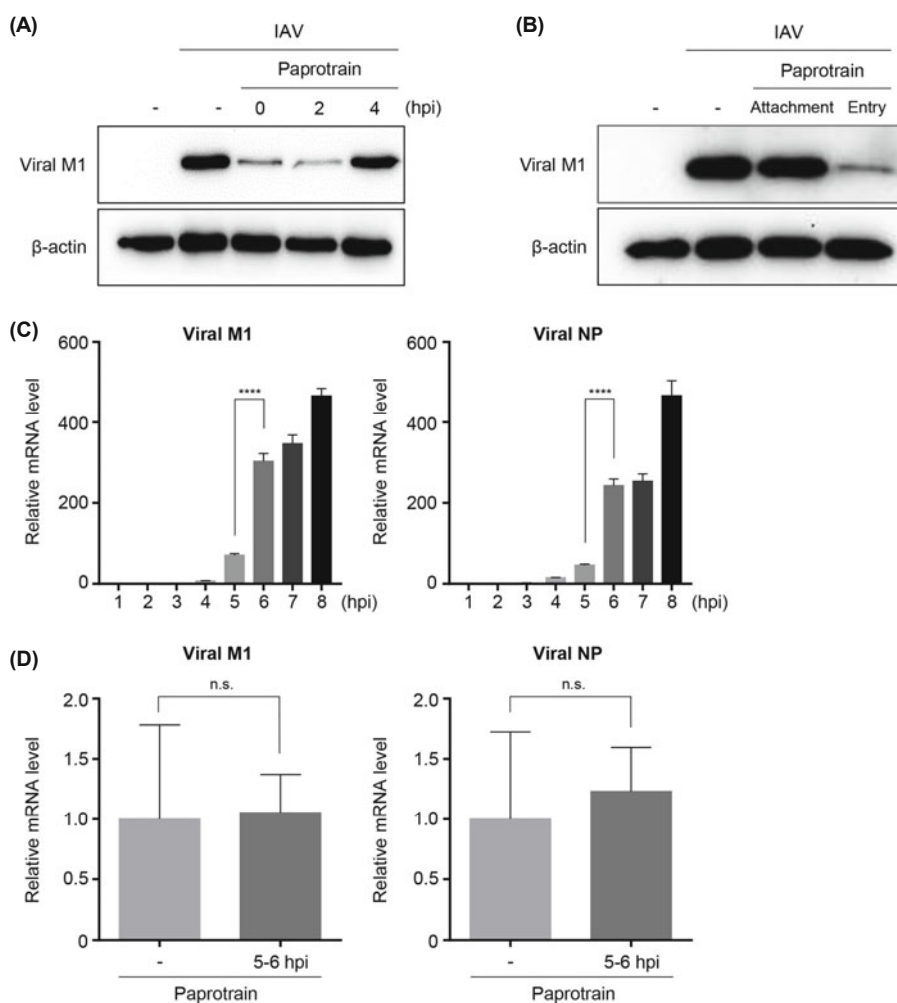


Fig. 5. Inhibition of KIF20A interferes with the early entry process of IAV infection. HEK-293 cells were treated with paprotrain at a 2.5 µg/ml concentration. (A and B) The cells were infected with IAV at an MOI of 1. (A) The cells were treated with paprotrain at 0, 2, or 4 hpi and then further incubated up to 20 hpi. The expressions of viral M1 and β-actin were analyzed by western blotting. (B) For the Attachment, cells were incubated with IAV in the presence of paprotrain at 4°C for 1 h. For the Entry, cells were infected with IAV for 1 h, followed by immediate treatment with paprotrain for 2 h. Cells were harvested at 20 hpi and the expressions of viral M1 and β-actin were analyzed by western blotting. (C and D) Cells were infected with IAV at an MOI of 0.1, and viral M1 and NP mRNA levels were quantified by qRT-PCR. (C) Relative mRNA levels were analyzed at each time point after IAV infection. (D) Cells were treated with paprotrain at 5 hpi for 1 h (5–6 hpi). The relative transcription levels of viral M1 and NP are shown. Statistically significant differences between samples were identified via Student's *t*-test (*****P* < 0.0001). All experiments were conducted at least three times.

affects the activity of IAV RNA-dependent RNA polymerase (RdRP), which transcribes viral negative (-) RNA strands into positive (+) RNA strands. Since (+) RNAs of viral M1 and NP were dramatically increased between 5 and 6 hpi, we treated IAV-infected cells with paprotrain at 5 hpi for 1 h (Fig. 5C). However, paprotrain did not significantly reduce

the transcription level of viral M1 and NP (i.e., viral mRNA level) (Fig. 5D), indicating that KIF20A does not affect the IAV RdRP activity. These data suggest that KIF20A might be involved in the entry process rather than viral attachment and viral RNA synthesis.

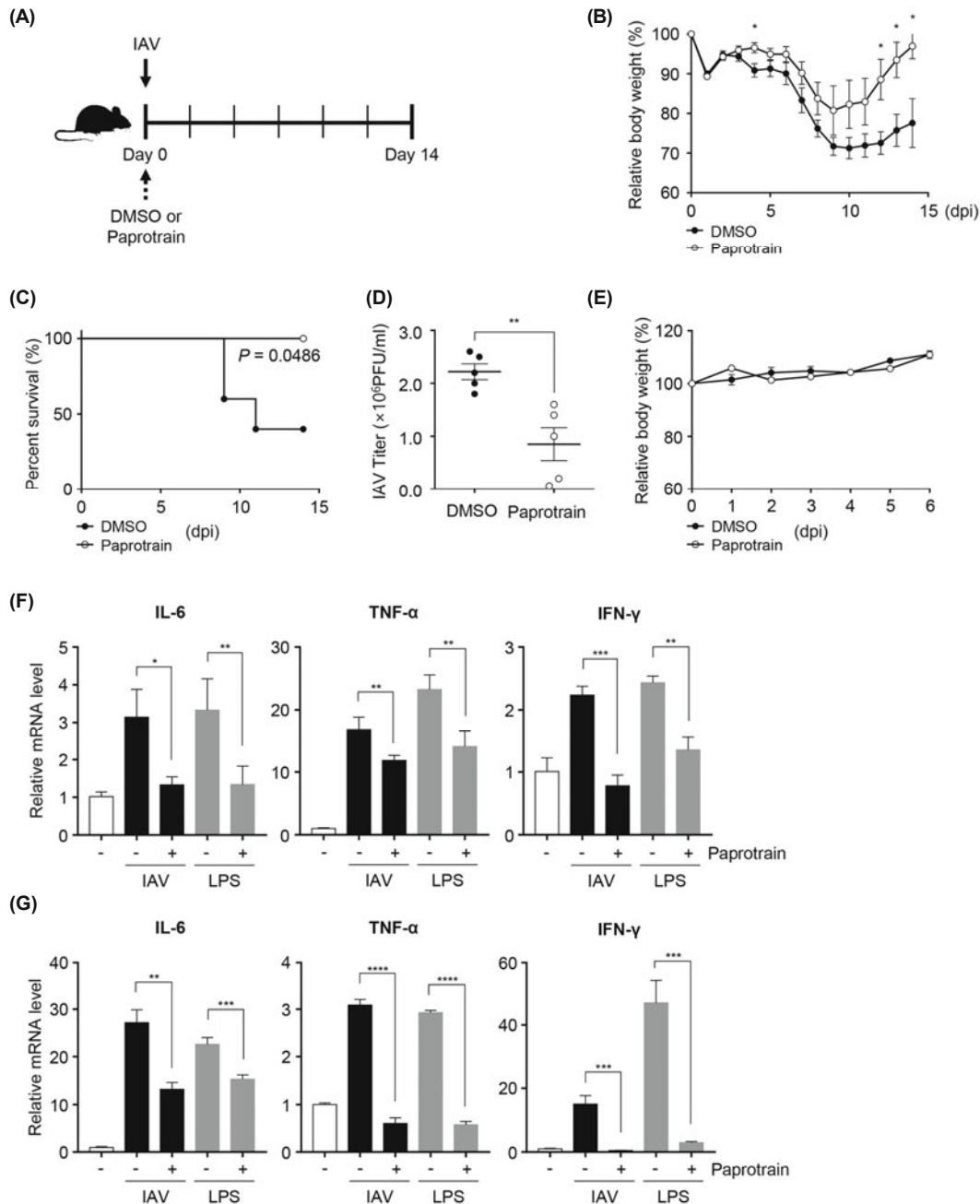


Fig. 6. Paprotrain protected mice from IAV-induced morbidity and mortality. (A) 7- to 8-week-old C57BL/6 wild type mice were infected with IAV and treated with DMSO (control) or paprotrain (0.0025 mg/kg). (B) Relative body weights measured for 14 days. The open circle plot represents the paprotrain-treated group ($n = 5$) and the filled circle plot represents the DMSO-treated group (CTR) ($n = 5$). (C) The percent survival of mice is depicted for each group. P -values were obtained using a log-rank test. (D) Mice were sacrificed at 5 dpi to obtain viral titers in lungs via the plaque assay. (E) Relative body weights of DMSO- or paprotrain-treated mice measured for 6 days are shown. (F and G) Lung cells and splenocytes isolated from wild type C57BL/c mice were stimulated with IAV or LPS in the presence or absence of paprotrain (5 μ g/ml). (F) The relative mRNA expression levels of IL-6, TNF- α , and IFN- γ in lung cells are shown. (G) The relative mRNA expression levels of IL-6, TNF- α , and IFN- γ in splenocytes are shown. Statistically significant differences between samples were determined via unpaired Student's t -test (* $P < 0.05$, ** $P < 0.01$, *** $P < 0.001$, **** $P < 0.0001$). All experiments were conducted at least twice.

Paprottrain protects mice from IAV-induced morbidity and mortality

Considering the antiviral potential of paprottrain *in vitro*, we examined whether paprottrain could also have antiviral activity *in vivo*. Wild type C57BL/6 mice were intranasally infected with IAV, followed by treatment with DMSO or paprottrain (0.0025 mg/kg). Body weight and survival rate were measured for 14 days (Fig. 6A). Paprottrain-treated mice exhibited less weight loss and faster weight recovery compared to the control group (Fig. 6B) with an increased survival rate (Fig. 6C). Furthermore, paprottrain treatment greatly reduced the pulmonary viral burden compared to DMSO-treated mice at 5 dpi (Fig. 6D). However, administration of paprottrain without IAV infection did not result in any morbidity including body weight loss (Fig. 6E). Finally, we investigated whether paprottrain treatment affects the expression of inflammatory cytokines including IL-6, TNF- α , and IFN- γ , which are known to be associated with disease severity in patients (Liu *et al.*, 2016). To this end, mouse lung cells and splenocytes isolated from wild C67BL/6 mice were infected with IAV in the presence or absence of paprottrain. Interestingly, paprottrain significantly reduced the transcription levels of IL-6, TNF- α , and IFN- γ in IAV-infected lung cells (Fig. 6F) and splenocytes (Fig. 6G). Furthermore, when LPS-stimulated lung cells or splenocytes were treated with paprottrain in the absence of IAV, the transcription level of inflammatory cytokines (TNF- α , IL-6, IFN- α) was also significantly decreased (Fig. 6F and G). Thus, the anti-inflammatory activity of paprottrain along with the anti-IAV activity could ameliorate IVA-associated symptoms and complications, which possibly contributes to the protection of mice from IAV-infected morbidity and mortality. Collectively, these results suggest that inhibition of KIF20A could be a novel antiviral strategy to treat IAV infection.

Discussion

In this study, we demonstrated that KIF20A is a proviral factor promoting IAV replication, and therefore its inhibition suppresses viral replication *in vitro* as well as *in vivo*. Importantly, we found that KIF20A plays a role in the early stages of IAV replication. Because viral entry is the first essential step of virus replication, this phase is an ideal target to efficiently block the viral infection. For example, the viral entry inhibitors enfuvirtide and Trimeris are clinically used to treat HIV infection (Esté and Telenti, 2007). Moreover, novel entry inhibitors are crucial in the current efforts to develop next generation anti-influenza drugs (Edinger *et al.*, 2014). Our results confirmed that paprottrain, a KIF20A inhibitor, inhibits the IAV entry step, and therefore this inhibitor could be used as an effective anti-IAV drug. Furthermore, discovering other KIF20A inhibitors could also contribute to the development of novel anti-IAV drugs. Although we focused on the anti-influenza activity of KIF20A, this inhibitor could also be used to treat other types of viruses, which require further investigation.

Although there are several vaccines and antiviral drugs available for the prevention and treatment of influenza virus (Nicholson *et al.*, 2000; Hong *et al.*, 2021), the constant emer-

gence of new viral variants limits their application. Therefore, the development of new antiviral drug candidates and identification of their antiviral mechanisms are critical to control influenza infections. Given that respiratory viruses replicate in epithelial cells of the respiratory tract, intranasal treatment could be more effective to control these viruses. In our *in vivo* study, intranasal administration of paprottrain was shown to increase the survival rate and decrease the morbidity of IAV-infected mice. Although further safety tests are required, intranasal administration of paprottrain to mice without infection did not cause any significant morbid symptoms (Fig. 6E). Therefore, paprottrain could be developed as an intranasal drug for treatment of IAV-infected patients.

Several KIFs such as KIF13A, KIF11, and KIF18A are known to play diverse roles in IAV replications (Ramos-Nascimento *et al.*, 2017; Cho *et al.*, 2020; Kim *et al.*, 2021). Since KIFs are central components of the intracellular transport system, inhibition of KIFs might interfere with the transport of viral components, which is critical for IAV replication. When IAV-infected cells were treated with paprottrain at early times post infection (0–2 hpi), the expression of viral proteins was dramatically reduced (Fig. 5B). This indicates that paprottrain attenuates the early entry of IAV. However, viral attachment and RdRP activity were not affected by paprottrain treatment. Therefore, KIF20A-controlled microtubule dynamics are likely involved in the viral entry of IAV. However, additional studies are required to confirm this.

In conclusion, our study demonstrated that KIF20A is a proviral factor that regulates the early entry of IAV propagation. Given that paprottrain (a KIF20A inhibitor) strongly protected mice from IAV-induced mortality and morbidity, the inhibition of KIF20A could be an effective strategy for the treatment of IAV infection.

Acknowledgements

This study was supported by the National Research Foundation of Korea (NRF) grant funded by the Korean government [grant number: NRF-2018R1A5A1025077, 2021R1F1-A1047001, 2021R1I1A1A01041639].

Conflict of Interest

The authors declare that they have no competing interests.

Ethical Statement

All animal experiments were performed in accordance with protocols approved by the Institutional Animal Care and Use Committee of Ewha Womans University (Approval No.: EWHA MEDIACUC 22-020).

References

Brandenburg, B. and Zhuang, X.J. 2007. Virus trafficking—learning from single-virus tracking. *Nat. Rev. Microbiol.* 5, 197–208.

- Cho, Y.B., Hong, S., Kang, K.W., Kang, J.H., Lee, S.M., and Seo, Y.J. 2020. Selective and ATP-competitive kinesin KIF18A inhibitor suppresses the replication of influenza A virus. *J. Cell. Mol. Med.* **24**, 5463–5475.
- Dodding, M.P. and Way, M. 2011. Coupling viruses to dynein and kinesin-1. *EMBO J.* **30**, 3527–3539.
- Döhner, K., Nagel, C.H., and Sodeik, B. 2005. Viral stop-and-go along microtubules: taking a ride with dynein and kinesins. *Trends Microbiol.* **13**, 320–327.
- Edinger, T.O., Pohl, M.O., and Stertz, S. 2014. Entry of influenza A virus: host factors and antiviral targets. *J. Gen. Virol.* **95**, 263–277.
- Esté, J.A. and Telenti, A. 2007. HIV entry inhibitors. *Lancet* **370**, 81–88.
- Fukuyama, S. and Kawaoka, Y. 2011. The pathogenesis of influenza virus infections: the contributions of virus and host factors. *Curr. Opin. Immunol.* **23**, 481–486.
- Geng, A., Qiu, R., Murai, K., Liu, J., Wu, X., Zhang, H., Farhoodi, H., Duong, N., Jiang, M., Yee, J., et al. 2018. KIF20A/MKLP2 regulates the division modes of neural progenitor cells during cortical development. *Nat. Commun.* **9**, 2707.
- Greber, U.F. and Way, M. 2006. A superhighway to virus infection. *Cell* **124**, 741–754.
- Hong, S., Chang, J., Jeong, K., and Lee, W. 2021. Raloxifene as a treatment option for viral infections. *J. Microbiol.* **59**, 124–131.
- Kim, D.I., Kang, J.H., Kim, E.H., and Seo, Y.J. 2021. KIF11 inhibition decreases cytopathogenesis and replication of influenza A virus. *Mol. Cell. Toxicol.* **17**, 201–212.
- Kim, H., Webster, R.G., and Webby, R.J. 2018. Influenza virus: dealing with a drifting and shifting pathogen. *Viral Immunol.* **31**, 174–183.
- Labrière, C., Lozach, O., Blairvacq, M., Meijer, L., and Guillou, C. 2016a. Further investigation of paprotrain: towards the conception of selective and multi-targeted CNS kinase inhibitors. *Eur. J. Med. Chem.* **124**, 920–934.
- Labrière, C., Talapatra, S.K., Thoret, S., Bougeret, C., Kozielski, F., and Guillou, C. 2016b. New MKLP-2 inhibitors in the paprotrain series: design, synthesis and biological evaluations. *Bioorg. Med. Chem.* **24**, 721–734.
- Lim, Y.S., Mai, H.N., Nguyen, L.P., Kang, S.M., Tark, D., and Hwang, S.B. 2021. Adenosylhomocysteinase like 1 interacts with non-structural 5A and regulates hepatitis C virus propagation. *J. Microbiol.* **59**, 101–109.
- Liu, J., Wang, Q.C., Cui, X.S., Wang, Z.B., Kim, N.H., and Sun, S.C. 2013. MKlp2 inhibitor paprotrain affects polar body extrusion during mouse oocyte maturation. *Reprod. Biol. Endocrinol.* **11**, 117.
- Liu, Q., Zhou, Y., and Yang, Z. 2016. The cytokine storm of severe influenza and development of immunomodulatory therapy. *Cell. Mol. Immunol.* **13**, 3–10.
- Louw, J.J., Nunes Bastos, R., Chen, X., Verdood, C., Corveleyn, A., Jia, Y., Breckpot, J., Gewillig, M., Peeters, H., Santoro, M.M., et al. 2018. Compound heterozygous loss-of-function mutations in *KIF20A* are associated with a novel lethal congenital cardiomyopathy in two siblings. *PLoS Genet.* **14**, e1007138.
- Luo, M. 2012. Influenza virus entry. *Adv. Exp. Med. Biol.* **726**, 201–221.
- Miki, H., Setou, M., Kaneshiro, K., and Hirokawa, N. 2001. All kinesin superfamily protein, KIF, genes in mouse and human. *Proc. Natl. Acad. Sci. USA* **98**, 7004–7011.
- Nakamura, M., Takano, A., Thang, P.M., Tsevegjav, B., Zhu, M., Yokose, T., Yamashita, T., Miyagi, Y., and Daigo, Y. 2020. Characterization of KIF20A as a prognostic biomarker and therapeutic target for different subtypes of breast cancer. *Int. J. Oncol.* **57**, 277–288.
- Nicholson, K.G., Aoki, F.Y., Osterhaus, A.D., Trottier, S., Carewicz, O., Mercier, C.H., Rode, A., Kinnersley, N., and Ward, P. 2000. Efficacy and safety of oseltamivir in treatment of acute influenza: a randomised controlled trial. *Lancet* **355**, 1845–1850.
- Noh, K., Jeong, E.J., An, T., Shin, J.S., Kim, H., Han, S.B., and Kim, M. 2022. The efficacy of a 2,4-diaminoquinazoline compound as an intranasal vaccine adjuvant to protect against influenza A virus infection *in vivo*. *J. Microbiol.* **60**, 550–559.
- Qiu, X., Wu, S., Hilchey, S.P., Thakar, J., Liu, Z.P., Welle, S.L., Henn, A.D., Wu, H., and Zand, M.S. 2015. Diversity in compartmental dynamics of gene regulatory networks: the immune response in primary influenza A infection in mice. *PLoS ONE* **10**, e0138110.
- Radtke, K., Döhner, K., and Sodeik, B. 2006. Viral interactions with the cytoskeleton: a hitchhiker's guide to the cell. *Cell. Microbiol.* **8**, 387–400.
- Ramos-Nascimento, A., Kellen, B., Ferreira, F., Alenquer, M., Vale-Costa, S., Raposo, G., Delevoye, C., and Amorim, M.J. 2017. KIF13A mediates trafficking of influenza A virus ribonucleoproteins. *J. Cell Sci.* **130**, 4038–4050.
- Shen, T., Yang, L., Zhang, Z., Yu, J., Dai, L., Gao, M., Shang, Z., and Niu, Y. 2019. KIF20A affects the prognosis of bladder cancer by promoting the proliferation and metastasis of bladder cancer cells. *Dis. Markers* **2019**, 4863182.
- Ward, B.M. 2011. The taking of the cytoskeleton one two three: how viruses utilize the cytoskeleton during egress. *Virology* **411**, 244–250.
- Wu, W.D., Yu, K.W., Zhong, N., Xiao, Y., and She, Z.Y. 2019. Roles and mechanisms of Kinesin-6 KIF20A in spindle organization during cell division. *Eur. J. Cell Biol.* **98**, 74–80.
- Zhang, Q., Di, J., Ji, Z., Mi, A., Li, Q., Du, X., Wang, A., Wang, A., and Qin, C. 2020. KIF20A predicts poor survival of patients and promotes colorectal cancer tumor progression through the JAK/STAT3 signaling pathway. *Dis. Markers* **2020**, 2032679.
- Zhang, Y., Liu, J., Peng, X., Zhu, C.C., Han, J., Luo, J., and Rui, R. 2014. KIF20A regulates porcine oocyte maturation and early embryo development. *PLoS ONE* **9**, e102898.
- Zhu, Z., Jin, Z., Zhang, H., Zhang, M., and Sun, D. 2020. Knockdown of *Kif20a* inhibits growth of tumors in soft tissue sarcoma *in vitro* and *in vivo*. *J. Cancer* **11**, 5088–5098.